Chiral bipolar colloids from nonchiral chromonic liquid crystals

A. Nych,[1,2] U. Ognysta,[1,2] I. Muševič,[2,3] D. Seč,[3] M. Ravnik,[3] and S. Žumer[2,3]
[1]*Institute of Physics, prospect Nauky, 46, Kyiv 680028, Ukraine*
[2]*J. Stefan Institute, Jamova 39, 1000 Ljubljana, Slovenia*
[3]*Faculty of Mathematics and Physics, University of Ljubljana, Jadranska 19, 1000 Ljubljana, Slovenia*
(Received 15 November 2013; published 9 June 2014)

We demonstrate that high anisotropy of elastic constants of chromonic liquid crystals leads to a number of spontaneously twisted nematic director fields around colloidal particles in these non-chiral fluids. For spherical colloidal particles with surface inducing degenerate planar nematic ordering we observe that boojum defects at the particles' poles acquire twisted internal structure, extending up to three particle diameters along the rubbing direction of the cell. The twist handedness of the two boojum defects at the poles of the particle can be either the same or opposite, and we can switch the defects handedness by localized thermal microquenching. Numerical simulations confirm that the transitions into the distorted states are induced by lowering of the twist elastic constant, which results in two (meta)stable chiral configurations of the boojums, separated by an energy barrier much higher than the thermal energy. We show that boojum handedness can change the pairwise elastic interaction between the two particles positioned along the rubbing direction from repulsive to attractive.

DOI: 10.1103/PhysRevE.89.062502 PACS number(s): 61.30.−v, 64.70.pv

I. INTRODUCTION

Lyotropic chromonic liquid crystals (LCLCs) are remarkable complex fluids, in which the elongated, rodlike clusters of small organic molecules, dissolved in water, are spontaneously aligned along the direction called the director **n**. The aggregation of these organic molecules is driven by soft attraction, resulting in a spontaneous formation of long stacks or clusters of nonmesogenic molecules, which eventually form liquid crystalline phase [1,2]. At the molecular level, the lyotropic chromonic liquid crystals are characterized by rather broad distribution of the lengths of these aggregates. At the macroscopic level, chromonic liquid crystals are similar to the conventional (molecular) liquid crystals. They are typically low-birefringent materials with the birefringence in the range from $\Delta n = 0.004$ to 0.1 and the elasticity of the chromonic LCs is similar to the elasticity of thermotropic nematic liquid crystals, with one exception. The macroscopic twisting of the chromonic LC turns out to be only weakly energetically penalized, resulting in a small twist elastic constant [3]. As a further motivation, chromonic lyotropic LCs exhibit complex interactions in between the molecules forming the aggregates and between the molecules of the aggregates and solvent (water) molecules [1,2,4–8]. It was recently demonstrated that chromonic liquid crystals are truly biocompatible [9]. They can host living organisms, which opens new directions towards active complex matter and biology.

A relatively steady development in the already mature field of liquid crystals (LCs) was inspired over the last decades primarily by their successful electro-optic applications in LCDs [10]. On the other hand, novel electro-optical applications have emerged, such as liquid crystal dispersions [11,12], where the liquid crystals can be either dispersed in an isotropic matrix (direct LC dispersion) or used as a host medium to disperse other materials (inverted LC dispersions). It has been found that solid particles dispersed in the nematic LC matrix exhibit complex effective pair interactions through the deformation field of the liquid crystal [13–15]. This interaction is long-ranged and very anisotropic, and can be used to assemble and stabilize various two-dimensional (2D) and 3D colloidal structures, including 2D and 3D nematic collodial crystals [16–18]. Whereas 2D and 3D nematic colloidal crystals could be used as photonic band-gap materials for photonic applications, aqueous or gel dispersions of LC microdroplets turned out to form another family of photonic materials, such as microlasers [19,20] and optical microresonators [21]. To obtain more complex photonic architectures using liquid crystals, it is important to develop new liquid crystalline materials that are not miscible with each other. Chromonic liquid crystals, which are based on aqueous solutions of organic molecules, are immiscible with usual thermotropic liquid crystals, and are therefore an interesting new class of LC materials for new photonic applications.

Chirality of liquid crystal matrix is known to induce interesting new effects in LC colloids. For example, the Saturn-ring colloids can form stable and chiral colloidal dimers in twisted LC cells [22] and several colloidal particles may be encircled with one or a few knotted or linked defect loops with nontrivial topological properties [23]. The helical structure of the cholesteric LCs is responsible for twisting and wrapping the Saturn-ring defects around homeotropic particles [24], which results in screening of the effective colloidal pair potential [25]. It also transforms the boojums on planar particles into twisted surface defects [26], forcing the rodlike particles to rotate when pushed perpendicularly to the cholesteric helical axis [27]. However, using twisted nematic cells or chiral nematic liquid crystals is not the only way to generate chiral configurations in liquid crystals. It is known that anisotropic elasticity of a nonchiral nematic LC can cause director configuration to be twisted even if the liquid crystal itself is not chiral.

For example, it was shown that the interior of a nematic LC droplet with a planar surface anchoring adopts either a bipolar (nonchiral) or twisted bipolar (chiral) director configuration, depending on the ratio of the elastic constants of the LC material [28,29]. The chiral configuration is formed when $K_1 \geqslant K_2 + 0.431K_3$ [29] and the LC prefers to spontaneously twist (elastic constant K_2) in order to relax the energy-costly

splay (K_1) or bend (K_3) deformations. This criterion requires that the elastic constants of liquid crystal should also satisfy the $K_3/K_1 < 1$ inequality [30]. These materials are relatively rare and hence special conditions are needed to realize the twisted bipolar configuration in LC droplets. This configuration was observed in a temperature region close to the nematic-to-smectic-*A* transition where the first inequality is satisfied [31], or by adding a small amount of a chiral dopant (not enough to fully induce cholesteric phase) to the LC matrix [32]. It was also reported by Stark [33] that for $K_2 < K_1$ the dipolar colloidal particle adopts twisted dipolar configuration. Another effect that could be used to explain the twisted director configuration in the nematic and also chromonic liquid crystals is the geometrical anchoring effect [4,34]. The chromonic liquid crystals are generally "soft" in the twist deformation, which means that chiral configurations of the chromonic LC are likely to occur in chromonic colloidal dispersions. This is the main motivation of our work presented in this paper.

Here we study the configuration of the chromonic LC around spherical solid particles or liquid droplets of an immiscible fluid with planar surface anchoring, dispersed in the lyotropic CLC matrix. In usual thermotropic LC matrix such particles have a bipolar director configuration with two boojum defects on their poles and interact as elastic quadrupoles [35–37]. In the LCLC material we observe that due to the low twist elastic constant, the pointlike boojums are accompanied by two long twisted tails extending up to two or three particle diameters along the cell rubbing direction. Interestingly, the two tails around the particle are rather independent, i.e., they may be twisted in the same direction or in opposite thus creating four possible director field configurations. The chirality of twisted tails also modifies the interparticle pair potential by an additional attractive or repulsive interaction along the rubbing direction depending on the twist handedness.

II. EXPERIMENT

We performed our experiments at room temperature (25 °C) with 15 wt % water solution of disodium cromoglycate (DSCG) lyotropic chromonic liquid crystal (also known as Cromolyn Sodium, Spectrum Chemical Mfg. Corp., $C_{23}H_{14}Na_2O_{11}$, 98% purity without further purification). At this concentration the solution exhibits the nematic phase within the 23–28 °C range [1,38].

All cells were prepared using 1 mm thick glass slides covered with rubbed SE-7511 polyimide layer (Nissan chemicals) for good planar alignment of DSCG, as described in Ref. [38]. The thickness of the cells was controlled by Mylar film spacers and was usually set to 30 μm, although in some cases the cells of ∼12 μm and ∼85 μm thickness were used. Two kinds of cromolyn-based colloids were prepared: (i) the emulsion of PVA-stabilized water droplets in cromolyn, and (ii) the dispersion of solid microspheres in cromolyn. For the emulsion preparation we mixed the cromolyn solution with 5 wt % water solution of polyvinyl alcohol (PVA, Sigma-Aldrich) with PVA to DSCG solution ratio of approximately 1:50, so the isotropic droplets of PVA-water solution were formed in the DSCG matrix. A similar technique was used in Ref. [39] to produce a direct emulsion of LCLC tactoids in the PVA-water solution.

The dispersion of solid particles in cromolyn was prepared by mixing the DSCG solution with 12 μm and 19 μm polystyrene or silica particles (Sigma-Aldrich). LCLC materials usually exhibit planar anchoring on most surfaces and it is rather difficult to achieve stable homeotropic anchoring in these systems [40]. Therefore the particles were not treated with any surface alignment layers and are assumed to have planar anchoring. The concentration of particles was experimentally adjusted to around ∼1 wt % to have them well separated from each other yet having a relatively dense colloidal dispersion. The cells were filled by dispersions or emulsions at room temperature by using the vacuum pump and were hermetically sealed with an epoxy glue to prevent water evaporation. All investigations were performed several hours after the cells were sealed, therefore allowing the cromolyn solution to equilibrate and establish a good alignment.

The colloidal particles were manipulated using the laser tweezers setup built around an inverted optical microscope (Nikon TE-2000) with 1064 nm cw laser controlled by a pair of acousto-optic deflectors (AOD, Aresis). A water immersion objective (60×, N.A. = 1.0) was used for manipulating colloidal particles during experiments. By applying a higher laser power we were able to locally heat the chromonic liquid crystal matrix into the isotropic phase and perform thermal quenching, when the laser was rapidly turned off.

III. DISCUSSION

A. Microscopic observations

Microscope images of colloidal dispersions of 12 or 19 μm polystyrene or silica particles in DSCG under crossed polarizers are shown in Fig. 1. From crossed-polarizer images in Fig. 1(a), one can immediately see that each particle has two elongated and birefringent "tails" in addition to four bright (and localized) sectors, that are characteristic for planar bipolar particles with surface boojum defects in thermotropic LCs [37]. These additional bright elongated tails start from the particles' surface and extend along the cell rubbing direction up to three particle diameters. Furthermore, by inserting the λ plate between crossed polarizers and the sample, local orientation of the director becomes visible as differently colored areas [41]. By analyzing Fig. 1(b), one can distinguish two differently colored tails, i.e., bluish and yellowish. Furthermore, we can notice that one of the two particles in Fig. 1(a) has both tails of the same color, whereas the second particle has differently colored tails. Similar elongated "tails" were recently observed by Lavrentovich [42].

These tails were also observed in the emulsion of PVA-stabilized water droplets in a DSCG matrix. Spherical liquid droplets have an advantage over solid particles because there is no preferred direction at the droplets' surfaces [43] which allows liquid crystal molecules (or aggregates in case of LCLC materials) to freely glide and rotate on the interface and the planar degenerate anchoring is automatically realized. In addition, the density of the PVA-stabilized water droplets is much closer to the density of the DSCG solution, so the

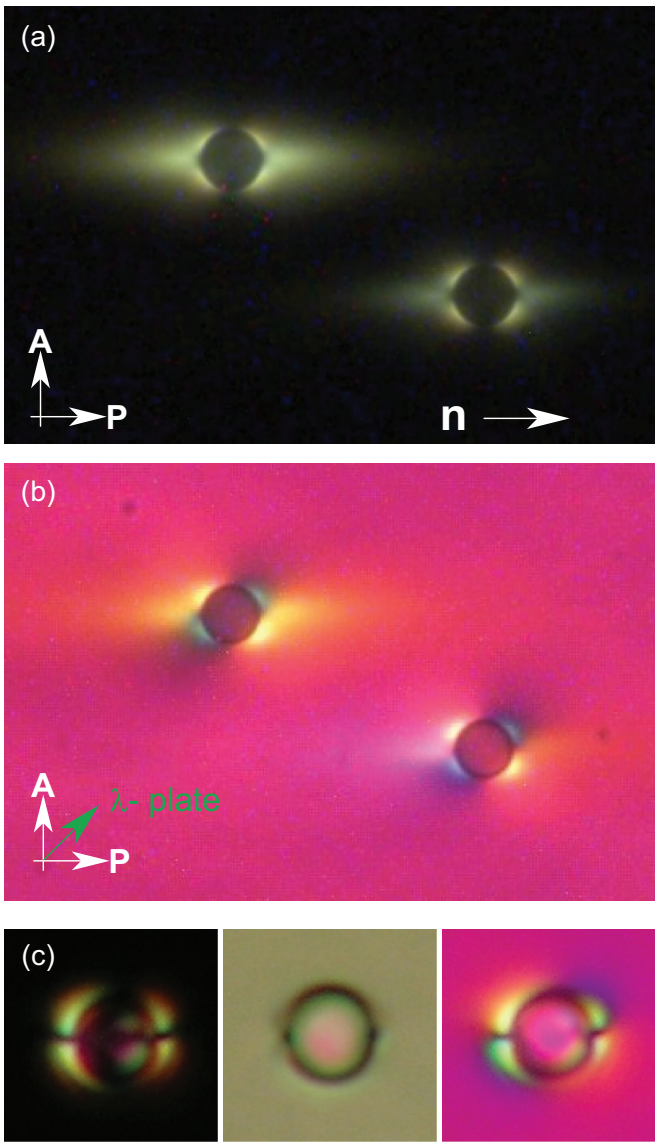

FIG. 1. (Color online) Microscope images of 12 μm polystyrene microspheres in the DSCG solution under (a) crossed polarizers and (b) crossed polarizers with a λ plate. Using the λ plate allows for the determination of local orientation of molecules; see Ref. [41]. Note two different colors of the cromolyn tails in (b). The cell thickness is 30 μm. (c) Images of 4.32 μm silica particles with planar surface alignment in 6 μm planar cell filled with 5CB liquid crystal. From left to right: crossed polarizers, no polarizers, crossed polarizers with the λ plate.

PVA-stabilized droplets float inside the cell. We therefore performed further analysis with the DSCG + PVA emulsion only, although most of the discovered features are common to the solid polystyrene and silica particles as well.

The DSCG + PVA emulsion shows polydispersity of droplet diameters, the size of droplets ranging from ∼1 μm to ∼15 μm [see Figs. 2(a) and 2(b)]. However, the droplets of PVA solution appear differently for different diameters. For droplets with diameters below ∼2.5–3 μm there are no visible birefringent areas around them because they are too small to cause noticeable deformation of the LCLC material. A similar effect was also observed for DSCG-based colloids with a critical size around ∼2 μm [6]. Larger PVA droplets with diameter up to ∼6–8 μm appear the same as planar quadrupolar particles in thermotropic LCs [37]; one can see four bright birefringent lobes around them. Finally, particles larger than ∼6–8 μm have additional long birefringent tails, as shown in Figs. 1 and 2. The brightness and length of their tails depend on the droplet size: larger droplets have brighter and longer tails. The length of the tails reaches up to three droplets' diameters (∼30–40 μm for ∼15 μm droplets).

We noted that the long tails have either bluish or yellowish colors under crossed polarizers with a λ wave plate aligned at 45° [see Fig. 2(c)]. It is not possible to make the tails completely dark only by rotating the cell between crossed polarizer and analyzer. The light, transmitted through the tails, is therefore no longer linearly polarized, but is elliptically polarized. This change in the state of polarization of transmitted light must be a consequence of highly nonuniform structure of the tails, which results in a rather strong structural birefringence due to its twisted structure. However, by rotating the polarizer (or the analyzer), it was indeed possible to partially darken the tails, but different parts of the tail were darkened at different orientations of the polarizer. This means that the main axis of the polarization ellipse of light, transmitted through the tails, is rotated, and the twisted tails act as weak polarization rotators. To characterize this rotatory power of the tails, we aligned the rubbing direction along the microscope analyzer (i.e., parallel to the horizontal axis of the image), rotated the microscope polarizer in steps of 10° and recorded consecutive images of the tails over the full angle of 360° [44]. Then the sequence of images was analyzed by extracting the light intensity from each pixel as a function of polarizer angle ϕ and this intensity was fitted to the $I \propto \sin(\phi - \phi_{\rm min}^{\rm eff})^2$ function. From this procedure we obtain a 2D map of minimal intensity orientation $\phi_{\rm min}^{\rm eff}(x,y)$ of the polarizer as a function of x and y image coordinates, which gives us the information on the rotation of polarization of light, distribution over the imaged sample area.

Figure 2(d) shows the distribution of recovered angle of effective rotation of light polarization $\phi_{\rm min}^{\rm eff}(x,y)$ using the described technique for the same area, as shown in Figs. 2(a)–2(c). Far from the particles we indeed observe that $\phi_{\rm min}^{\rm eff}(x,y) \simeq 0$, while in the tails near the particle we see that the LC director must be substantially twisted with the maximal detected effective twist angle around 15–20°. A similar technique was used to determine the twist angle in the LC droplets or tactoids [4,11,30], although there are some subtle, but important, differences in the optics of twisted tactoids and twisted tails in our experiments.

It should be noted that the angle of rotation of light polarization determined with this technique may not correspond to the actual twist angle of the nematic director in the cell. Namely, it relies upon the fact that in the twisted LC sample the polarized light travels through the LC in the Mauguin regime [45], where the polarization of light follows the LC director and rotates together with it. This regime is realized in the LC sample when $\lambda \ll P|\Delta n|/2$ [45] (P is the LC director pitch, Δn is the LC birefringence, and λ is the wavelength of light). There

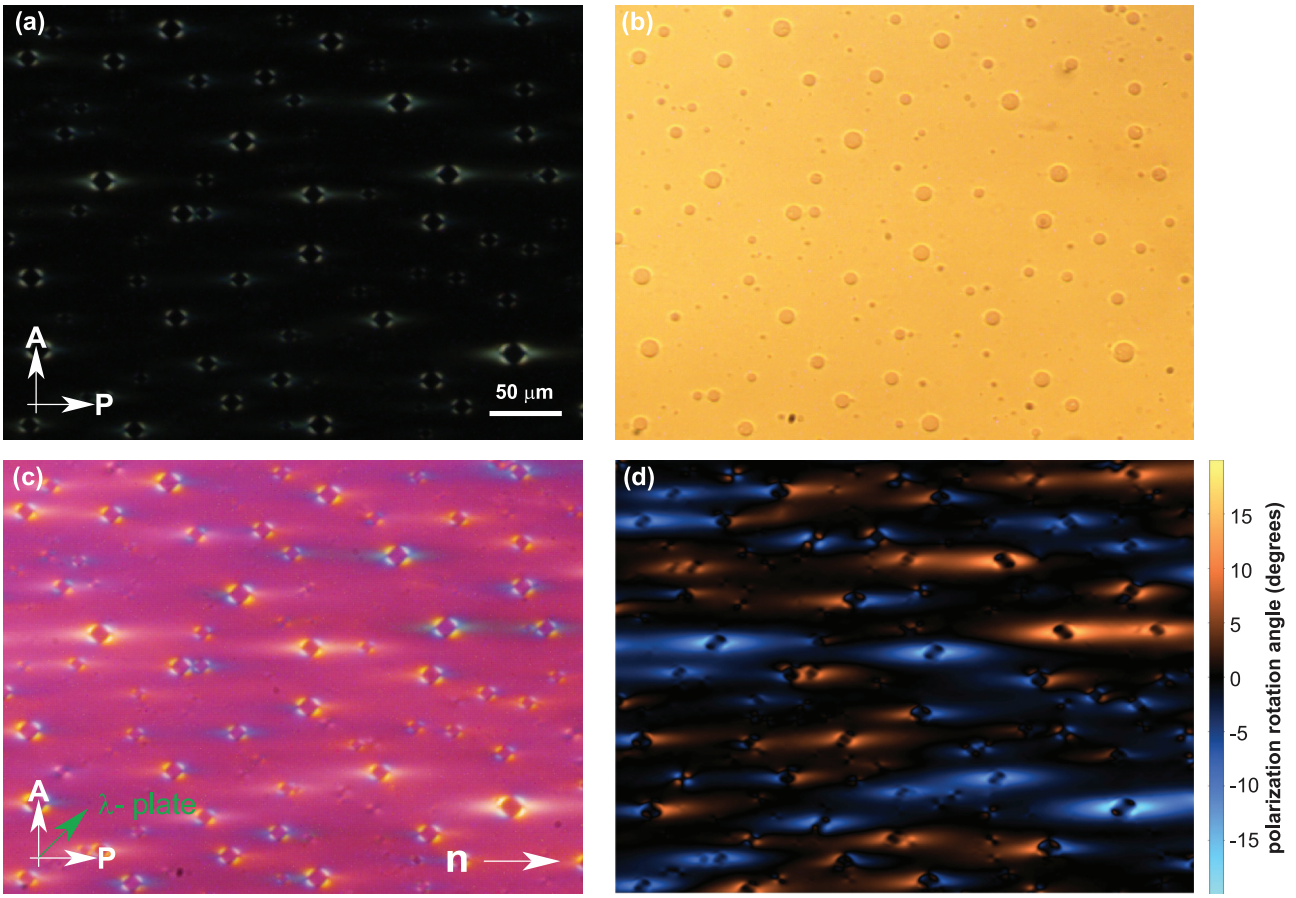

FIG. 2. (Color online) Microscopic photographs of PVA-stabilized water droplets in DSCG lyotropic chromonic liquid crystal matrix: (a) under crossed polarizers; (b) under normal illumination; (c) under crossed polarizers with a λ wave plate inserted between the polarizer and the sample. Note that droplets larger than ∼6–8 μm have bright long tails oriented along the cell rubbing direction. (d) The map of the angle of effective rotation of light polarization, recovered from a series of images recorded during the rotation of the polarizer. The cell thickness is 30 μm.

are two factors suggesting that the Mauguin regime might not be realized in our samples. First, the birefringence of the DSCG chromonic liquid crystal is small, $\Delta n_{DSCG} \approx -0.02$ [38], that significantly lowers the right side of the inequality. Second, the director distribution in the tails cannot have only a pure uniform twist along the normal to the cell (perpendicular to the image plane), but has a more complex twisted structure, where it is difficult to define the pitch P. A more detailed analysis of the twisted tail optics will be given further on in this text based on computer simulated director profiles.

By comparing Figs. 2(c) and 2(d) one can notice that bluish and yellowish colors of the tails in Fig. 2(c) correspond to the opposite sense of the twist of the LC director. This means that the tails are chiral objects and that both chiralities of the tails can be observed in the experiments on solid particles (see Fig. 1) and liquid droplets in DSCG chromonic liquid crystal (see Fig. 2). A careful analysis of the images reveals that if a particle has equally twisted tails they appear slightly wider as if they were oppositely twisted.

We observed four different configurations around twisted bipolar colloids in the DSCG chromonic liquid crystal matrix depending on the twisting direction of their tails: left-left and right-right (LL, RR) and left-right and right-left (LR, RL). Collecting statistics from the rather polydisperse PVA-stabilized water droplets in DSCG LCLC, we observe an approximately equal number of LL and RR configurations, whereas the number of configurations with oppositely twisted tails is somewhat lower, which indicates a higher free energy of these configurations. More specifically, the probability for finding a structure with the same handedness (LL or RR) is ∼60%, whereas the probability for finding a structure with opposite handedness (LR or RL) is ∼40%. To ensure that chiral tails do not appear as a result of the confinement of the colloids by the cell walls, we prepared different cells of thickness up to ∼85 μm with PVA solution droplets and still observed all four possible combinations of the twisted tails around the droplets.

Using a strong localized light of the laser tweezers we were able to switch the chirality of a selected tail. By focusing a high power laser beam of laser tweezers at the twisted tail we heated the chromonic LC material into the isotropic phase around the laser focus. When the laser was turned off the molten liquid crystal cooled down very fast and again formed a chiral tail configuration. The twist direction after cooling was random, regardless of the initial state. By changing the laser power we were able to switch either one twisted tail or even both of them if the laser power was high enough to melt the LCLC around the whole particle into the isotropic phase. The configuration

created in this way was stable over the whole duration of our experiments.

B. Pair interaction of colloids with chiral tails

The fact that the director field around the planar colloids in LCLC is chiral should have a strong influence on the interaction of a colloidal pair, which should depend on the pair chirality [46,47]. The experiments indeed confirm this conjecture. We observe that two colloids attract each other, when the neighboring tails of two interacting particles have the same chirality, and we observe repulsion when the chirality of the tails is opposite. This is illustrated in Fig. 3, which shows the time evolution of the interaction of three droplets. The two colloids that are not aligned exactly along the rubbing direction show an attraction, which is characteristic to the attraction of quadrupolar particles in the thermotropic LCs. Here the maximum of attraction is at $\sim 30^\circ$ with respect to the rubbing direction [35,36].

Initially [Fig. 3(a)] the droplet on the left and the droplet in the middle are aligned along the direction of strongest attraction. They attract each other [Figs. 3(b) and 3(c)] and finally merge into a bigger drop [Fig. 3(d)]. During the coalescence their inner tails disappear and the newly formed droplet inherits its tails from the remaining outer tails of the parent pair. Now the new droplet (as well as the original middle one) and the droplet on the right are aligned exactly along the rubbing direction and have their inner tails twisted in the same direction. They also attract each other [Figs. 3(e) and 3(f)] and finally merge too. By using the laser tweezers we also aligned a pair of particles with oppositely twisted neighboring tails along the rubbing direction, which were close enough to cause overlapping of their tails. When the laser tweezers was switched off, the particles started to move away from each other to avoid the overlapping of oppositely twisted tails.

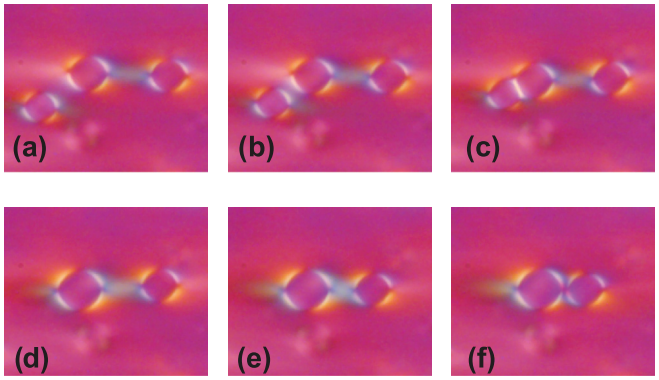

FIG. 3. (Color online) Snapshots of the attraction and coalescence of PVA-stabilized water droplets in the DSCG chromonic liquid crystal matrix observed under crossed polarizers with λ wave plate. The two particles on the left and in the center attract each other (a)–(c) at $\sim 30^\circ$ with respect to the rubbing direction (as planar quadrupolar particles do in the thermotropic LCs [36]) and finally merge into a bigger droplet (d). The remaining pair attracts each other along the rubbing direction (d–f), because the chiralities of their interacting inner tails (and their color) are the same.

C. Numerical simulations and results

To analyze our experiments in more detail we performed numerical modeling of the LC configuration around planar bipolar particles using a mean field Landau–de Gennes free energy approach, based on full tensorial order parameter Q_{ij}. The free energy F [48] is constructed from the invariants of Q_{ij} allowed by symmetry to account for the variation of nematic degree of order, elastic distortions, and surface anchoring contributions. The free energy reads [49]

$$\begin{aligned} F = & \int_{LC} \left\{ \frac{A}{2} Q_{ij} Q_{ij} + \frac{B}{3} Q_{ij} Q_{jk} Q_{kl} + \frac{C}{4} (Q_{ij} Q_{ij})^2 \right\} dV \\ & + \int_{LC} \left\{ \frac{L_1}{2} \frac{\partial Q_{ij}}{\partial x_k} \frac{\partial Q_{ij}}{\partial x_k} + \frac{L_2}{2} \frac{\partial Q_{ij}}{\partial x_j} \frac{\partial Q_{ik}}{\partial x_k} \right. \\ & \left. + \frac{L_3}{2} Q_{ij} \frac{\partial Q_{kl}}{\partial x_i} \frac{\partial Q_{kl}}{\partial x_j} \right\} dV \\ & + \int_{\Sigma} \{ W (\tilde{Q}_{ij} - \tilde{Q}^{\perp}_{ij})(\tilde{Q}_{ij} - \tilde{Q}^{\perp}_{ij}) \} d\Sigma, \end{aligned} \tag{1}$$

where the summation over repeated indices is assumed. A, B, and C are the nematic material parameters, L_1, L_2, and L_3 are the tensorial elastic constants connected to Frank-Oseen elastic constants for splay, $K_1 = \frac{9}{4} S^2 (2L_1 + L_2 - L_3 S)$, twist, $K_2 = \frac{9}{4} S^2 (2L_1 - L_3 S)$, and bend, $K_3 = \frac{9}{4} S^2 (2L_1 + L_2 + 2L_3 S)$ [50,51]. W is the surface anchoring strength and $\tilde{Q}_{ij}$ and $\tilde{Q}^{\perp}_{ij}$ are related to the full tensorial parameter, as defined by Fournier and Galatola [52]. The first two terms are integrated over the bulk of liquid crystal (LC) and the last term is integrated over the surface of the colloidal particle (Σ). This free energy is then numerically minimized according to the Euler-Lagrange partial-differential equations on a cubic grid [53] with a mesh resolution of 10 nm. The surface of colloidal particles is modeled as a thin shell of mesh points with the thickness equal to mesh resolution.

The elementary units of the LCLC material are aggregates floating in water [1,2] rather than molecules and hence the elasticity, viscosity, and other properties of these materials are quite different from those of the thermotropic LCs. Since we are interested in the equilibrium states, the most significant material property is the anisotropic elasticity, more precisely an unconventionally low twist elastic constant compared to the splay and bend constants [3]. To model the LCLC material, we thus used different elastic constants for splay, twist, and bend deformations. We used the following values for the tensorial constants: $L_1 = 4 \times 10^{-12}$ N, $L_2 = 7.9 \times 10^{-11}$ N, and $L_3 = 0$, giving the Frank-Oseen elastic constants $K_1 = K_3 = 5.2 \times 10^{-11}$ N and $K_2 = K_1/10 = 5.2 \times 10^{-12}$ N. The following material parameters were used in our simulations: $A = -0.172 \times 10^6$ J m^{-3}, $B = -2.12 \times 10^6$ J m^{-3}, $C = 1.73 \times 10^6$ J m^{-3}, $W = 1 \times 10^{-3}$ J m^{-2} [53]. These values correspond more to a standard thermotropic nematic liquid crystal [52] and are only qualitatively appropriate for LCLCs. Measurements of selected material parameters of LCLCs are reported in Refs. [3,54–57].

As expected from experiments, two possible bipolar director structures are found around the particle: (i) structure with the same and (ii) structure with opposite twist handedness of the two boojums, as presented in Figs. 4(a)–4(c) and 4(d)–4(f),

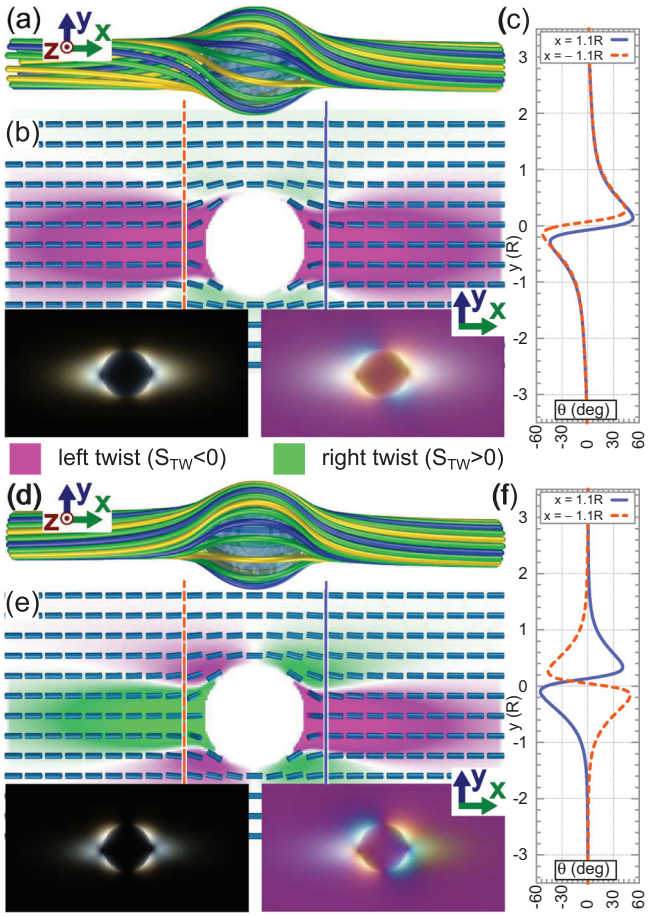

FIG. 4. (Color online) The results of computer simulations for planar particles with twisted boojums for the (a)–(c) chiral structure with same twist handedness and for (d)–(f) nonchiral structure with opposite twist handedness of the tails. (a),(d) Director field around the particle presented as 3D field lines, colored to guide the eye [note the (a) same and (d) opposite twisting of the streamlines]. (b),(e) xy plane ($z = 0$) cross section of the director field through the center of the particle and calculated transmission images under crossed polarizers (left) and under crossed polarizers with a λ wave plate (right). The images are cropped in y direction to focus on the configuration around the colloidal particle. (c),(f) Twist θ along the two indicated lines in (b),(e): solid plot for the solid line (right, blue), dashed plot for the dashed one (left, orange).

respectively. The simulated structures show small variations (up to 5% of the bulk value) in the nematic degree of order (mostly only at the particle surfaces) and can thus be to a very good approximation solely characterized only by the director profile. The director profiles are inherently scale free; therefore, the calculated structures can be scaled [49]. We have confirmed this conjecture also by simulating different sizes of the system: we scaled the simulation box together with the colloidal particle up to eight times in each direction and compared the obtained director fields. The characteristic director profiles stayed approximately the same for both structures, with maximal changes being less than 10%. This allowed us to speed up the simulations by using a simulation volume $3\times3\times1\,\mu\text{m}^3$ with particle diameter $2R = 0.6\,\mu$m. For the transmission image simulations we scaled the configurations uniformly to the desired cell thickness (usually $30\,\mu$m).

One can distinguish between the twisted structures by using the twist parameter that measures the twist deviation from the unperturbed state and is for the achiral nematic phase ($q_0 = 0$) defined as [58]

$$S_{TW} = \varepsilon_{ikl} Q_{ij} \frac{\partial Q_{lj}}{\partial x_k}, \tag{2}$$

and is measured in the units of inverse nematic correlation length ξ^{-1}. Rewriting the twist parameter from the Q_{ij} parametrization into the director dependence, and assuming uniform nematic degree of order, this term is proportional to the twist term in Frank elastic theory $\vec{n} \cdot (\nabla \times \vec{n})$.

To compare the simulated structures with polarization micrographs, shown in Figs. 2(a) and 2(c), we calculate the polarization micrographs using the Jones 2×2 matrix formalism [59] and taking the birefringence data for 15 wt % DSCG solution from [38]. The polarization micrographs for the the same- and opposite-twisted structures are shown in Figs. 4(b) and 4(e). In calculations, we use the "straight ray approximation" [59] by only accounting for the locally variable birefringence of the nematic refractive index and neglecting reflections and refractions on interfaces. In this approach, the beam is propagated along a chosen direction and phase shifts between the ordinary and extraordinary rays are being calculated. The procedure is then repeated for ten different wavelengths in the approximate radiation spectra of the black body at 6000 K (i.e., white light approximation) and converted to the sRGB color space using the standard color matching functions [60].

The calculated transmission images in Figs. 4(b) and 4(e) qualitatively match the experimental photographs presented in Figs. 1 and 2. The bright tails observed in the experiments between crossed polarizers are the areas in which twist of the boojum defects gradually diminish along the cell rubbing direction and eventually turn into the uniform director field of the planar cell. Images with crossed polarizers and λ wave plate show tails having different colors and also widths according to their twist handedness, exactly as observed in experiments. The twist handedness is visualized with the twist parameter S_{TW} [see Figs. 4(b) and 4(e)] that distinguishes between the left-handed twist ($S_{TW} > 0$, green) and the right-handed ($S_{TW} < 0$, violet). The twist parameter is highest at the surface of the particle along the rubbing direction of the cell and diminishes with the distance from the particle. Speculatively, one could further affect the twist by adding a chiral dopant to the LCLC. First, this would bias the configuration with the same handedness as the dopant by making it energetically more favorable. And second, having sufficiently high concentration of the chiral dopant, the intrinsic pitch induced by the dopant could be enforced in the colloidal system and, possibly, structures as observed in chiral (thermotropic) nematic liquid crystal colloids could emerge [24,61].

Now we can analyze optics of the twisted tails using the simulated LC director profiles. We scaled the simulated director profiles to the experimental cell thickness $H = 30\,\mu$m and followed the polarization ellipse orientation along the light path using Jones matrix formalism. In order to

analyze Mauguin regime in the cell we estimated "local" Mauguin parameter $M_{\rm local}(x,y,z) = P_{\rm local}(x,y,z)|\Delta n|/(2\lambda)$ where $P_{\rm local}(x,y,z)$ is a local equivalent to pitch defined as $P_{\rm local}(x,y,z) = 2\pi/(\frac{\partial\theta(x,y,z)}{\partial z})$ (distance on which director would rotate by 2π turning with the local rate $\partial\theta(x,y,z)/\partial z$). We observe that the local Mauguin parameter decreases from $\simeq 75$ at the substrate to $\simeq 10$ after light travels $\simeq 2$–$2.5\ \mu$m in the LC. The further the light travels through the cell the faster the LC director rotates and the lower is $M_{\rm local}$, reaching $\simeq 0.1$ in the middle of the cell where the LC director changes its rotation direction to opposite and returns back to the initial twisting direction in approximately $\simeq 6\ \mu$m. Thus we see that the Mauguin regime in the cell is lost after light propagates just a few microns in the LC and linearly polarized incident light quite quickly becomes elliptically polarized and orientation of the long axis of the polarization ellipse does not correlate with the director rotation, especially when the light leaves the cell.

Our calculations, based on the Jones matrix approach, demonstrate that DSCG-filled cell of $30\,\mu$m thickness with simulated director profiles effectively rotates polarization (or long axis of the polarization ellipse) by approximately $\pm(15-30)^\circ$ depending on the initial polarization orientation with respect to the rubbing direction, where the sign depends on the twist direction of the tail. Thus, the $15-30^\circ$ angle of polarization rotation is the angle we detected in our experiments and its magnitude is far from the actual maximal director deviation $\sim 55-60^\circ$ from the rubbing direction. This behavior is very close to the experimental results, presented in Fig. 2(d), where the polarization rotation angle in the tails measured at the similar distance from the center of the particle is $\approx 10-15^\circ$.

The simulations were performed without introducing additional parameters to take into account the specific material properties of lyotropic chromonic LCs, which suggests that chiral boojums may be realized also in usual thermotropic LC, similarly, as the predicted twisted dipole configurations around collodial particles in thermotropic LCs [33]. To explore the effect of the twist elastic constant on the chirality of the nematic director configurations, we varied the ratio of the splay to twist elastic constant $\alpha = K_1/K_2$. For used parameters, the twisted boojums were obtained if the elastic constant anisotropy was larger than the critical $\alpha_c = K_1/K_2 = 2$. Notably, the boojum tail lengths exhibit a critical behavior (Fig. 5), following $l_t \sim (\alpha - \alpha_c)^\beta$ with the exponent $\beta = 0.34 \pm 0.01$ for $R = 0.3\ \mu$m particles. We tested this critical ratio using numerical simulations. First, we find that α_c is dependent on the particle size. For example, for smaller particles ($R = 0.1\ \mu$m) we observe no tails at $\alpha = 2$ and only much shorter tails ($\sim 3\times$ shorter) at $\alpha = 3$. And second, we observe hysteresis in the region close to the critical ratio. If α is increased, for $R = 0.3\ \mu$m particles, the long tails emerge at $\alpha \approx 2.25$ and gradually increase in length with increasing α. However, if decreasing α, the tails become short already at $\alpha < 2.5$, being four times shorter at $\alpha = 2.25$ as compared to when increasing the α ratio.

The tail length is defined as the distance in the rubbing direction of the cell at which the twist parameter is notably large, i.e., $|S_{TW}| > 0.01$. For $K_1/K_2 \leqslant 2$ the tail length is approximately zero and at $K_1/K_2 = 2$ the transition to the twisted state occurs. The tail length then grows with the increased ratio of the elastic constants. For $K_1/K_2 \sim 10$ the tail length is $\sim 3R$, similar to what is observed in the experiments. The twisted tails also vanish when surface anchoring is lower than $W_c \sim 5\times 10^{-5}$ J/m^2 for $R = 0.3\ \mu$m particles. From the experimental observation that the twisted tails only become visible at particles with $R_c \gtrsim 6\ \mu$m, we can estimate [62] the experimental value of the surface anchoring at particle surface as $W^{(\rm exp)} = W_c \frac{R}{R_c} \sim 2.5\times 10^{-6}$ J/m^2. This is similar to the estimates in Refs. [40,56].

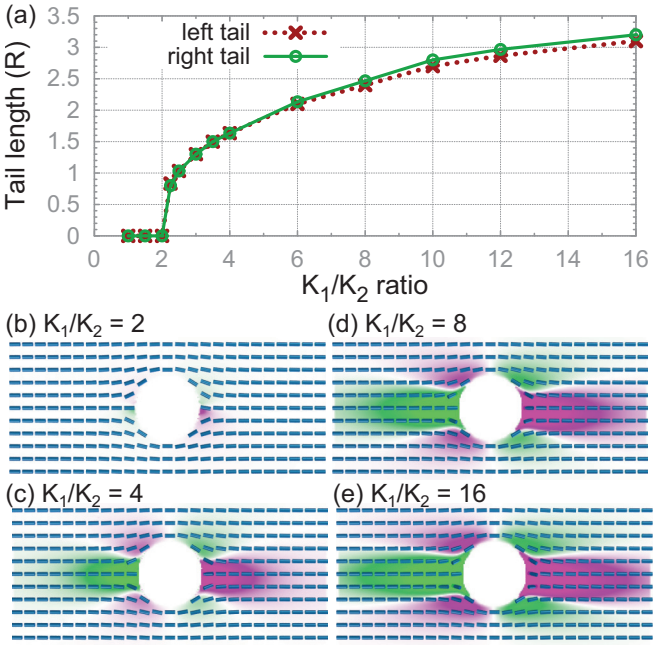

FIG. 5. (Color online) The length of the twisted tails (i.e., regions where $|S_{TW}| > 0.01$) in the boojum defects exhibits a second-order phase transition at elastic constant anisotropy $K_1/K_2 = 2$ for $R = 0.3\ \mu$m particles. The length of the tails can be as long as few particle diameters. (b)–(e) Twist parameter visualized for different K_1/K_2 ratios. Note the increasingly larger green ($S_{TW} > 0.01$) and violet ($S_{TW} < -0.01$) areas upon increasing the K_1/K_2 ratio.

The total free energy of the configuration with the same twist handedness of the tails—scaled for colloidal particle of $2R = 12\,\mu$m as $E_s \sim \frac{r_{\rm exp}}{r_{\rm mod}} E \sim 20E$—is $E_{LL} = E_{RR} \simeq 1.582\times 10^{-15}$ J. The free energy difference of the configuration with opposite twist handedness of the tails is $\Delta E_{LR} = E_{LR} - E_{LL} \simeq 6000\, k_B T$, identifying the opposite-handed structures (LR and RL) as strongly metastable. This is in agreement with experimental results, since the same-twisted structure is observed more frequently. In same- and opposite-twisted structures the director field is generally well ordered in the preferred direction with only some elastic deformations (mainly twist) in the vicinity of the particles. To estimate the energy barrier separating the two configurations we calculated the free energy E_{0R} of an imaginary configuration with the twisted boojum structure on one side of the particle and a nontwisted boojum on the other side, $\Delta E_{0R} = E_{0R} - E_{LL} \simeq 36\,000\, k_B T$. This is four orders of magnitude higher than the thermal energy and this explains why a spontaneous

transition from the L+R to L+L configuration is never observed.

In order to better visualize the equilibrium director configuration near the boojum defects, we extracted a horizontal cross section of the director field cutting through the center of the simulation box, parametrizing the director along the specified directions as $\vec{n} = (\cos\psi\cos\theta, \sin\psi, \cos\psi\sin\theta)$. The cross section is presented in Figs. 4(b) and 4(e) along with two director twist angle profiles θ extracted along two lines from both sides of the particle [Figs. 4(c) and 4(f)]. One can see that in the central region [see Figs. 4(c) and 4(f)] the LC director rotates strongly in one direction, whereas outside of this region the LC director rotates only weakly in the opposite direction resulting in a zigzag shape of the θ profile. The strong rotation of the LC director near the boojum defect (near the middle of the cell) is caused by the interplay of splay, twist, and bend deformations generated by the boojum. The LC director twists in order to minimize the energy penalty, similarly as in twisted bipolar LC drops [28,29], in a geometrical anchoring effect in wedge-shaped cells [34], and in tactoids [4]. The zigzag shape of the θ profile appears because, regardless of the twist direction near the boojum defect, the LC director has to align along the rubbing direction (along the x axis) on the substrates, which can be achieved only through opposite handedness of the twist.

According to our simulation results the LC director twist angle θ in the equilibrium configuration reaches its maximal value (almost $\pm 90^\circ$) in the close vicinity of the boojum defects. Such a large value of θ near the twisted boojums can be explained by very strong anisotropic elasticity of lyotropic chromonic liquid crystal materials. Recent results for the sunset yellow LCLC [3] show that the twist elastic constant K_2 is more than one order of magnitude smaller compared to splay K_1 and bend K_3 elastic constants, exactly in line with our modeling results, whereas in usual thermotropic LCs the ratio $K_{1,3}/K_2 \simeq 1.5-2$ is much smaller [63]. Although reliable measurements of elastic constants of DSCG material are still needed, the elastic constants and especially their ratios should be comparable to those of sunset yellow material due to general similarity between their internal structure [1,2]. The sunset yellow LCLC material has higher splay and bend elastic constants compared to 5CB liquid crystal, for example. However, the twist elastic constant of the sunset yellow is smaller compared to 5CB. Thus, strong anisotropic elasticity results in a high energy penalty of the splay and bend deformations near each boojum defect and low twist elastic constant facilitates twist generation as a possible way to relax the costly splay and bend deformations. That is why we see maximal twist deformations near the boojum defects.

An additional mechanism that is specific for LCLC and allows high-energy deformations to relax stems from the elementary building blocks of chromonic mesophases. Usual LC materials are monomolecular substances or mixtures of anisometric rod- or disk-like molecules which may be partially flexible but never break apart. In contrast, the LCLC materials are formed through noncovalent reversible aggregation of organic molecules in water [1,2]. Their building blocks are aggregates which float in the solvent. They are dynamic objects [64] and their length distribution may change in response to temperature changes [65] or deformations [40]. These aggregates may also rearrange themselves and locally alter their length distribution thus changing their elastic properties locally in response to strong elastic deformations that are generated near the boojum defect. In a rigid rod model which is only qualitatively appropriate for LCLCs [3], the elastic constants scale equally with the rod length L as $K_i \sim L^4$ [66], indicating that shorter aggregate lengths would roughly equally lower all elastic constants. This mechanism of elastic strain relaxation cannot be realized in conventional thermotropic LCs, but in the case of chromonic liquid crystals it may further decrease the energy penalty of splay and bend deformations near defects.

IV. CONCLUSIONS

In this paper we present experimental and numerical studies of formation of twisted bipolar configuration around colloidal particles with planar degenerate surface anchoring in nonchiral chromonic liquid crystal matrix, as caused by high anisotropic elasticity of the LC. Such director configurations around spherical colloids under crossed polarizers appear as bright long tails extending from the particle surface along the rubbing direction of the cell. The two twisted boojums of the same particle can be of the same or opposite handedness thus creating four possible director configurations around a single particle. Configurations with the same twist handedness (left-left or right-right) are the stable ones while energy of the metastable configurations with opposite twist handedness (left-right or right-left) is calculated to be $6000\,k_bT$ higher for 12 μm particles. We estimate that energy barrier separating the stable same-handed and metastable opposite-handed states is around $36\,000\,k_bT$, preventing a spontaneous transition between the two states. Measuring the length of the twisted tails gives the insight to the splay to twist elastic constant anisotropy and by observing the critical disappearance of the distortion with the reducing of the particle size the surface anchoring strength is estimated.

The nontwisted bipolar colloids interact as elastic quadrupoles, having four attractive directions symmetrically at an angle to the cell rubbing direction. Lowering the twist elastic constant compared to the splay and bend constants changes the interparticle potential depending on the twist handedness of the tails of neighboring particles. We observe that the particles attract each other also along the cell rubbing directions when the neighboring boojums have the same twist handedness and repel otherwise. This opens new routes to control particle interaction potential and tailoring new LC colloidal structures.

ACKNOWLEDGMENTS

The work was supported by NAS of Ukraine via Grant No. 1.4.B/162 and Slovenian ARRS Grants No. P1-0099 and No. Z1-5441. M.R. acknowledges partial funding from EU FP7 MC Grant No. FREEFLUID. A.N. and U.O. acknowledge helpful discussion with V. Nazarenko and D.S. acknowledges helpful discussions with S. Čopar.

[1] J. Lydon, J. Mater. Chem. **20**, 10071 (2010).
[2] J. Lydon, Liq. Cryst. **38**, 1663 (2011).
[3] S. Zhou, Y. A. Nastishin, M. M. Omelchenko, L. Tortora, V. G. Nazarenko, O. P. Boiko, T. Ostapenko, T. Hu, C. C. Almasan, S. N. Sprunt, J. T. Gleeson, and O. D. Lavrentovich, Phys. Rev. Lett. **109**, 037801 (2012).
[4] L. Tortora and O. Lavrentovich, Proc. Natl. Acad. Sci. USA **108**, 5163 (2011).
[5] T. Sergan, T. Schneider, J. Kelly, and O. Lavrentovich, Liq. Cryst. **27**, 567 (2000).
[6] S. V. Shiyanovskii, T. Schneider, I. I. Smalyukh, T. Ishikawa, G. D. Niehaus, K. J. Doane, C. J. Woolverton, and O. D. Lavrentovich, Phys. Rev. E **71**, 020702 (2005).
[7] Y. Bae, H. Yang, S. Shin, K. Jeong, and M. Lee, J. Mater. Chem. **21**, 2074 (2011).
[8] S. Park, S. Kim, D. Kim, S. Kang, S. Shin, S. Kuo, S. Hwang, S. Lee, M. Lee, and K. Jeong, Adv. Funct. Mater. **21**, 2129 (2011).
[9] S. Zhou, A. Sokolov, O. D. Lavrentovich, and I. S. Aranson, Proc. Natl. Acad. Sci. USA **111**, 1265 (2014).
[10] D. Yang and S. Wu, *Fundamentals of Liquid Crystal Devices* (John Wiley & Sons, Chichester, 2006).
[11] P. S. Drzaic, *Liquid Crystal Dispersions* (World Scientific, New Jersey, 1995).
[12] Q. Li, *Liquid Crystals Beyond Displays: Chemistry, Physics, and Applications* (Wiley, New York, 2012).
[13] P. Poulin, H. Stark, T. Lubensky, and D. Weitz, Science **275**, 1770 (1997).
[14] T. C. Lubensky, D. Pettey, N. Currier, and H. Stark, Phys. Rev. E **57**, 610 (1998).
[15] B. I. Lev and P. M. Tomchuk, Phys. Rev. E **59**, 591 (1999).
[16] I. Muševič, M. Skarabot, U. Tkalec, M. Ravnik, and S. Žumer, Science **313**, 954 (2006).
[17] U. Ognysta, A. Nych, V. Nazarenko, M. Skarabot, and I. Muševič, Langmuir **25**, 12092 (2009).
[18] A. Nych, U. Ognysta, M. Škarabot, M. Ravnik, S. Žumer, and I. Muševič, Nat. Commun. **4**, 1489 (2013).
[19] M. Humar and I. Muševič, Opt. Express **18**, 26995 (2010).
[20] M. Humar and I. Muševič, Opt. Express **19**, 19836 (2011).
[21] M. Humar, S. Pajk, M. Ravnik, and I. Muševič, Nat. Photon. **3**, 595 (2009).
[22] U. Tkalec, M. Ravnik, S. Žumer, and I. Muševič, Phys. Rev. Lett. **103**, 127801 (2009).
[23] U. Tkalec, M. Ravnik, S. Čopar, S. Žumer, and I. Muševič, Science **333**, 62 (2011).
[24] V. S. R. Jampani, M. Škarabot, M. Ravnik, S. Čopar, S. Žumer, and I. Muševič, Phys. Rev. E **84**, 031703 (2011).
[25] V. S. R. Jampani, M. Škarabot, S. Čopar, S. Žumer, and I. Muševič, Phys. Rev. Lett. **110**, 177801 (2013).
[26] J. S. Lintuvuori, K. Stratford, M. E. Cates, and D. Marenduzzo, Phys. Rev. Lett. **105**, 178302 (2010).
[27] D. Engstrom, R. Trivedi, M. Persson, M. Goksor, K. Bertness, and I. Smalyukh, Soft Matter **7**, 6304 (2011).
[28] G. Volovik and O. Lavrentovich, Sov. Phys. JETP **58**, 1159 (1983).
[29] R. Williams, J. Phys. A **19**, 3211 (1986).
[30] P. Drzaic, Liq. Cryst. **26**, 623 (1999).
[31] O. Lavrentovich and V. Sergan, Nuovo Cimento D **12**, 1219 (1990).
[32] Z. Lu and D. Yang, Appl. Phys. Lett. **65**, 505 (1994).
[33] H. Stark, Eur. Phys. J. B **10**, 311 (1999).
[34] O. D. Lavrentovich, Phys. Rev. A **46**, R722 (1992).
[35] P. Poulin and D. A. Weitz, Phys. Rev. E **57**, 626 (1998).
[36] I. I. Smalyukh, O. D. Lavrentovich, A. N. Kuzmin, A. V. Kachynski, and P. N. Prasad, Phys. Rev. Lett. **95**, 157801 (2005).
[37] U. M. Ognysta, A. B. Nych, V. A. Uzunova, V. M. Pergamenschik, V. G. Nazarenko, M. Skarabot, and I. Muševič, Phys. Rev. E **83**, 041709 (2011).
[38] Y. A. Nastishin, H. Liu, T. Schneider, V. Nazarenko, R. Vasyuta, S. V. Shiyanovskii, and O. D. Lavrentovich, Phys. Rev. E **72**, 041711 (2005).
[39] K. Simon, P. Sejwal, R. Gerecht, and Y. Luk, Langmuir **23**, 1453 (2007).
[40] V. G. Nazarenko, O. P. Boiko, H.-S. Park, O. M. Brodyn, M. M. Omelchenko, L. Tortora, Y. A. Nastishin, and O. D. Lavrentovich, Phys. Rev. Lett. **105**, 017801 (2010).
[41] U. Tkalec, M. Škarabot, and I. Muševič, Soft Matter **4**, 2402 (2008).
[42] O. D. Lavrentovich, Soft Matter **10**, 1264 (2014).
[43] M. Kleman and O. Lavrentovich, *Soft Matter Physics. An Introduction* (Springer, New York, 2003).
[44] Polarizing microscopes usually have their analyzer glued at some angle with respect to the optical axis in order to prevent multiple reflections in optical system. Due to this analyzer rotation causes image shift thus making quantitative analysis of sequence of images difficult.
[45] P. Yeh and C. Gu, *Optics of Liquid Crystal Displays* (John Wiley & Sons, New York, 1999).
[46] V. M. Pergamenshchik and V. A. Uzunova, Phys. Rev. E **83**, 021701 (2011).
[47] O. M. Tovkach, S. B. Chernyshuk, and B. I. Lev, Phys. Rev. E **86**, 061703 (2012).
[48] P. de Gennes and J. Prost, *The Physics of Liquid Crystals*, 2nd ed. (Oxford University Press, Oxford, UK, 1993).
[49] M. K. McCamley, G. P. Crawford, M. Ravnik, S. Žumer, A. W. Artenstein, and S. M. Opal, Appl. Phys. Lett. **91**, 141916 (2007).
[50] K. Schiele and S. Trimper, Phys. Status Solidi B **118**, 267 (1983).
[51] D. Seč, T. Lopez-Leon, M. Nobili, C. Blanc, A. Fernandez-Nieves, M. Ravnik, and S. Žumer, Phys. Rev. E **86**, 020705 (2012).
[52] J. B. Fournier and P. Galatola, Europhys. Lett. **72**, 403 (2005).
[53] M. Ravnik and S. Žumer, Liq. Cryst. **36**, 1201 (2009).
[54] A. V. Golovanov, A. V. Kaznacheev and A. S. Sonin, Izv. Ros. Akad. Nauk. Ser. Fiz. **59**, 82 (1995).
[55] A. V. Golovanov, A. V. Kaznacheev and A. S. Sonin, Izv. Ros. Akad. Nauk. Ser. Fiz. **60**, 43 (1996).
[56] Y. Li and N. A. Clark, Liq. Cryst. **40**, 1736 (2013).
[57] Y.-K. Kim, S. V. Shiyanovskii, and O. D. Lavrentovich, J. Phys.: Condens. Matter **25**, 404202 (2013).
[58] S. Copar, T. Porenta, V. S. R. Jampani, I. Muševič, and S. Žumer, Soft Matter **8**, 8595 (2012).
[59] R. Ondris-Crawford, E. P. Boyko, B. G. Wagner, J. H. Erdmann, S. Žumer, and J. W. Doane, J. Appl. Phys. **69**, 6380 (1991).
[60] H.-C. Lee, *Introduction to Color Imaging Science* (Cambridge University Press, New York, 2005).
[61] J. S. Lintuvuori, D. Marenduzzo, K. Stratford, and M. E. Cates, J. Mater. Chem. **20**, 10547 (2010).

[62] M. K. McCamley, M. Ravnik, A. W. Artenstein, S. M. Opal, S. Žumer, and G. P. Crawford, J. Appl. Phys. **105**, 123504 (2009).
[63] N. Madhusudana and R. Pratibha, Mol. Cryst. Liq. Cryst. **89**, 249 (1982).
[64] F. Chami and M. R. Wilson, J. Am. Chem. Soc. **132**, 7794 (2010).
[65] V. R. Horowitz, L. A. Janowitz, A. L. Modic, P. A. Heiney, and P. J. Collings, Phys. Rev. E **72**, 041710 (2005).
[66] J. P. Straley, Phys. Rev. A **8**, 2181 (1973).